Model for the Operation of a Monolayer MoS_2 Thin-Film Transistor with Charges Trapped near the Channel Interface

Ji-Hyun Hur,[1,*] Junghak Park,[1] Deok-kee Kim,[2] and Sanghun Jeon[1,†]

[1]*Department of Applied Physics, Korea University Sejong 2511, Sejong 339-700, Republic of Korea*
[2]*Electrical Engineering, Sejong University, 98 Gunja-dong, Gwangjin-gu, Seoul 143-747, Republic of Korea*

(Received 4 January 2017; revised manuscript received 15 March 2017; published 28 April 2017)

We propose a model that describes the operation characteristics of a two-dimensional electron gas (2DEG) in a monolayer transition-metal dichalcogenide thin-film transistor (TFT) having trapped charges near the channel interface. We calculate the drift mobility of the carriers scattered by charged defects located in the channel or near the channel interfaces. The calculated drift mobility is a function of the 2DEG areal density of interface traps. Finally, we calculate the model transfer ($I_D - V_{GS}$) and output ($I_D - V_{SD}$) characteristics and verify them by comparing with the experimental results performed with monolayer MoS_2 TFTs. We find the modeled results to be excellently consistent with the experiments. This proposed model can be utilized for measuring the interface-trapped charge and trap site densities from the measured transfer curves directly, avoiding more complicated and expensive measurement methods.

DOI: 10.1103/PhysRevApplied.7.044030

I. INTRODUCTION

In recent years, two-dimensional (2D) layered materials typified by graphene have attracted much attention due to their carrier mobilities, higher than that of silicon, originating from the lower effective masses of carriers. This high mobility property makes them suitable for substituting silicon in high-performance electronic devices. In addition to high carrier mobilities, 2D layered materials have advantages in transparency and in physical flexibility to expand their application range. Among 2D layered materials, transition-metal dichalcogenides (TMDCs) have also gained much interest owing to their relatively high carrier mobilities, finite band gaps (1–2 eV), which are normally not provided by a sheet of graphene, and high thermal stability required for applying them in high-performance field-effect transistors [1–10] or thin-film transistors (TFTs) [11,12]. Apart from the other advantages, high mobilities of TMDCs, e.g., up to 500 $cm^2/V\,s$ for bulk MoS_2 [13], make them increasingly attractive for use in TFTs, as the polysilicon- and oxide-based TFTs performances are limited by their carrier mobilities that are lower than approximately 100 $cm^2/V\,s$.

Monolayer TMDCs are considered to be more appropriate candidates among layered TMDCs for use in high-performance electronics because the effective masses of the carriers in monolayer TMDCs are smaller than those in multilayered TMDCs. Monolayer TMDCs are unique because of their nearly perfect two-dimensional nature. Therefore, the conventional transistor operation model [14] with either constant or field-dependent mobility cannot be applied. In the case of their application in TFTs as channel materials, carrier transport cannot be assumed ballistic for simplicity [1,15] due to the TFT channel lengths (a few micrometers) being much larger than a normal mean free path.

The key features of two-dimensional carrier transport in monolayer TMDC TFTs arise from the fact that the conducting carrier layer thickness is almost zero. This also makes the field-dependent mobility insignificant because the field effect results in narrowing the carrier layer thickness that affects scattering by charged traps near the channel boundaries and by roughness of the channel surface. Moreover, carrier scattering through these interface-related scattering mechanisms is maximized due to the proximity between the carriers and trapped charges near the interface that result in severe degradation of the carrier mobility. Several studies of the operational model of a TMDC metal-oxide-semiconductor field-effect transistor (MOSFET) with an ultrashort channel length that enables us to assume ballistic transport of carriers have been reported [1,15]. However, a model that can explain the transfer-curve characteristics of monolayer TMDC TFTs has not been reported so far.

In this paper, we present a theoretical model that describes the operational characteristics of monolayer TMDC TFTs with trapped charges near the channel interface which results in severe Coulomb scattering of carriers. This model aims to obtain the two-dimensional electron gas (2DEG) drift mobility through calculating the momentum relaxation rate of carriers in the frame of the Thomas-Fermi approximation [16] in the semiquantum Boltzmann transport formalism [17]. From the drift mobility, we can obtain

*Authors to whom all correspondence should be addressed. jhhur123@gmail.com
†jeonsh@korea.ac.kr

the drain current as a function of the gate bias (V_{GS}). In order to verify our model, we fabricate a TFT with a channel made up of monolayer MoS_2, which is the most widely used TMDC. Then we compare the experimentally measured transfer curves with the calculated results.

II. MODELING

To calculate the rate at which carriers are slowed down by the Coulomb field of the trapped charges toward the channel direction, we need to calculate the electric field produced by the trapped charges. First, we suppose a trapped charge is located at z from the 2DEG plane. Then, the Fourier-transformed Coulomb potential $V(q)$ due to the charge is given by [18]

$$V(q) = \frac{e^2}{2\varepsilon}\frac{e^{-qz}}{q+q_s}. \tag{1}$$

Here, q is the absolute value of the difference between the wave vector just before scattering and that after scattering, e is the unit charge of an electron, $\varepsilon = (\varepsilon_{ox} + \varepsilon_{MoS_2})/2$ is the averaged electrical permittivity of the channel and of the gate oxide, e is the absolute value of the unit charge, and q_s is the 2D screening parameter obtained using the 2D Thomas-Fermi screening theory that is a dimension of reciprocal length written as [18]

$$q_S = \frac{2\pi e^2}{\varepsilon}\frac{\partial n_{2D}}{\partial \mu} = \frac{2\pi e^2}{\varepsilon}\frac{gm^*}{\hbar^2\pi}\left[1-\exp\left(-\frac{\hbar^2\pi n_{2D}}{m^* k_B T}\right)\right], \tag{2}$$

where n_{2D} is the 2DEG areal density, μ is the Fermi potential, g is the degeneracy of the conduction-band minimum, which equals 2 for monolayer MoS_2 [19], $m*$ is the effective mass of electrons at the conduction-band minimum (K valley for monolayer MoS_2 [13]), k_B is the Boltzmann constant, and T is the absolute temperature.

Meanwhile, the momentum relaxation rate (the inverse of the momentum relaxation time) of 2DEG scattered by the interface-trapped charges located at distance z from the channel with density n_i is obtained by integrating over all the possible scattering events with weights of $1-\cos\theta$, where θ is the angle between the incident and scattered electrons as follows [20]

$$\frac{1}{\tau_{IT}} = n_{IT}\left(\frac{m^*}{2\pi\hbar^3 k_F^3}\right)\int_0^{2k_F}|V(q)|^2\frac{q^2 dq}{\sqrt{1-\left(q/2k_F\right)^2}}, \tag{3}$$

where τ_{IT} is the momentum relaxation time, n_{IT} is the areal density of charged interface traps, and k_F is the Fermi wave vector for 2DEG which equals $\sqrt{2\pi n_{2D}/g}$ [18]. Inserting Eq. (1) into Eq. (3) and assuming z is small and $q \ll q_s$, we obtain the momentum relaxation rate as

$$\frac{1}{\tau_{IT}} \cong n_{IT}\left(\frac{m^*}{2\pi\hbar^3 k_F^3}\right)\left(\frac{e^2}{2\varepsilon q_s}\right)^2\frac{(2k_F)^4}{6}\left(\frac{3\pi}{4k_F}-8z\right). \tag{4}$$

Trapped charges near the interface appear in various forms such as interface charges between the channel and its surroundings, oxide-trapped charges near the interface, and charges trapped by defects of the TMDC monolayer [19,21,22]. Thus, we define the effective thickness of the layer of trapped charges near the interface as the variable t, and then all these contributions should be taken into account in the calculation of momentum relaxation rate by integrating Eq. (4) in the z direction for the effective thickness of t as follows:

$$\frac{1}{t}\int_0^t 1/\tau_{IT}(z)dz = n_{IT}\left(\frac{m^*}{2\pi\hbar^3 k_F^3}\right)\left(\frac{e^2}{2\varepsilon q_s}\right)^2\frac{(2k_F)^4}{6}\left(\frac{3\pi}{4k_F}-4t\right). \tag{5}$$

To evaluate the average electron velocity in the channel direction, each electron velocity should be weighted using its distribution function. However, owing to the finite electric field in the channel direction due to the drain bias, electrons do not follow the Fermi-Dirac distribution function. Instead, the modified distribution function should be calculated to obtain the average carrier velocity. By solving Boltzmann's transport equation using the relaxation-time approximation for a weak electric field [17,23], the distribution function can be written as

$$f(k) = f_0(k) + \delta f(k) = f_0(k) - \frac{e}{\hbar}\tau(k)E_x\frac{\partial f_0(k)}{\partial k_x}, \tag{6}$$

where $f_0(k)$ is the equilibrium distribution function, E_x is the electric field in the channel (x) direction, and $\tau(k)$ is the mean free time between scatterings.

Then, the average electron velocity can be calculated by assuming that the incident electrons flow in the x direction ($k \sim k_x$) and taking k_F as the representative wave vector for the differential distribution function as follows [23]:

$$\langle v_x\rangle = \frac{\int_0^\infty v_x\delta f(k)dk}{\int_0^\infty f_0(k)dk} \cong \frac{e\hbar^2}{2(m*)^2 k_B T}\tau(k_F)k_F^2 E_x = E_x\mu_{drift}. \tag{7}$$

Inserting Eq. (5) into Eq. (7), we obtain the averaged carrier velocity in terms of the material and device parameters

$$\langle v_x\rangle = \frac{3\pi^{3/2}\hbar^5\varepsilon^2 q_s^2}{n_{IT}e^3(m*)^3 k_B T}\sqrt{\frac{n_{2D}}{2g}}\left(\frac{3\pi}{4}\sqrt{\frac{g}{2\pi n_{2D}}}-4t\right)^{-1}\frac{V_{SD}}{L} = \mu_{drift}E_x, \tag{8}$$

where μ_{drift} is the drift mobility assuming that electrons are scattered by the interface-trapped charges only.

Actually, electrons can be scattered by various kinds of scattering sources such as (acoustic or optical) phonon scatterings, piezoelectric scattering, and surface roughness scattering, etc. If we set μ_0 as the mobility calculated for all scattering sources (including the source and drain contact resistances) other than the interface-trapped charge scattering, then the electron drift mobility (μ_{tot}) is determined using Matthiessen's rule ($1/\mu_{\text{tot}} = 1/\mu_0 + 1/\mu_{\text{drift}}$). Thus, if the interface-trap scattering rate is much greater than the rates of other scattering processes, it determines the carrier transport in the TFT. It certainly is the case as compared with the lattice-scattering rate (ideal limit) in monolayer MoS_2 that shows a mobility of around 200 $\text{cm}^2/\text{V s}$ [8]. For the surface roughness scattering, although it depends on detailed processes, the mobility that is controlled by it is usually greater than approximately $100\,\text{cm}^2/\text{V s}$ [24]. Thus, we assume that if the drift mobility determined by the interface-trap scattering is much smaller than $100\,\text{cm}^2/\text{V s}$, it will solely determine the carrier transport regardless of the other scattering sources. At this stage, let us keep this assumption uncertain and confirm it by comparing the calculated and experimental results later in this paper.

III. RESULTS AND DISCUSSION

The drift mobilities calculated using Eq. (8) for different interface-trap densities are shown in Fig. 1. Except for the designed or given parameters, unknown parameters (n_{IT} and t) are selected to match the measured transfer curves that are fitted by the least-squares method, which we show later in this paper (Fig. 4). The 2DEG density range $[(5\times10^{10})$–$(2\times10^{12})\ \text{cm}^{-2}]$ corresponds to the calculated densities that equal $(V_{GS}-V_{\text{th}})C_{\text{ox}}/e$ (C_{ox} is the capacitance per unit area, which is the oxide permittivity per gate oxide thickness of $\varepsilon_{\text{ox}}/d$, and V_{th} is the threshold voltage) for the experimentally used gate overdrive range of 0–25 V. As can be seen in the figure, the drift mobility is proportional to the areal density of the carriers and inversely proportional to the interface-trap density. It is much smaller than the ideal mobility of monolayer MoS_2 (approximately 200 $\text{cm}^2/\text{V s}$) or the assumed criterion of 100 $\text{cm}^2/\text{V s}$. Thus, for these simulation parameters, we can safely assume that the drift mobility calculated from the scattering rates with interface-trapped charges represents the total drift mobility of electrons.

Finally, from the obtained relation of the carrier density and the average velocity [Eq. (8)], the drain current model that holds for both the linear and saturation regions can be expressed as [25]

$$I_D \cong e\mu_{\text{drift}}C_{\text{ox}}\frac{W}{L}\left[(V_{GS}-V_t)V_{SD}-\frac{1}{2}V_{SD}^2\right], \quad (9)$$

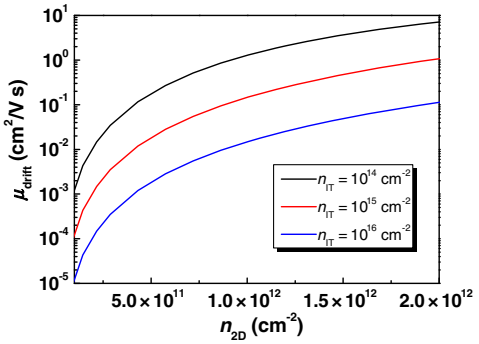

FIG. 1. The calculated drift mobility as a function of the 2DEG density for different interface-trapped charge densities.

where W and L are the width and the length of the channel, respectively, and V_{SD} is the voltage bias between the source and the drain. By inserting μ_{drift} in Eq. (8) into Eq. (9), we can finally obtain the drain current form in terms of detailed material and device properties.

To verify our model by comparing the calculated and experimental results, we fabricate a monolayer TMDC TFT, whose channel is monolayer MoS_2, and its schematic structure is shown in Fig. 2. A monolayer of MoS_2 is exfoliated from commercially available crystals of molybdenite (graphene market moly disulfide) using the Scotch-tape micromechanical cleavage technique pioneered for the production of graphene. A highly doped p-type silicon substrate is used for the gate electrode and to make the TFT channel. After Ti/Au contact deposition on top of the MoS_2 channels and the gate oxides, the devices are annealed in air. Next, for obtaining a passivating layer using a TEOS-based precursor, silicon oxide is prepared using sol-gel spin coating and the drying process at 85 °C. The microscopic top view of the fabricated TFT before the sol-gel passivation process is shown in Fig. 3. The inset of the figure is the Raman spectrum of the MoS_2 thin-film channel showing E^1_{2g} and A_{1g} peaks of monolayer MoS_2 [26]. The transfer-curve measurement scheme of the fabricated MoS_2 TFT is as follows. While the source (the voltage is 0 V) and the drain (the voltage is 1 or 10 V) biases are constant, the gate bias voltage changes from −30 to 30 V and back to −30 V. The transfer curves for the two voltage-sweep directions (from −30 to 30 V and from 30 to −30 V) differ due to the path dependence on charging effects. We choose the transfer curves of decreasing gate biases as the experimental curves for verifying the

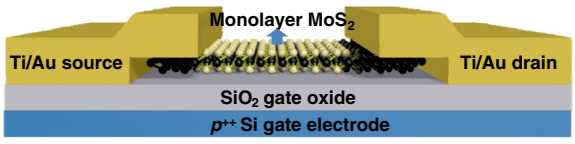

FIG. 2. Schematics of the monolayer MoS_2 thin-film transistor structure.

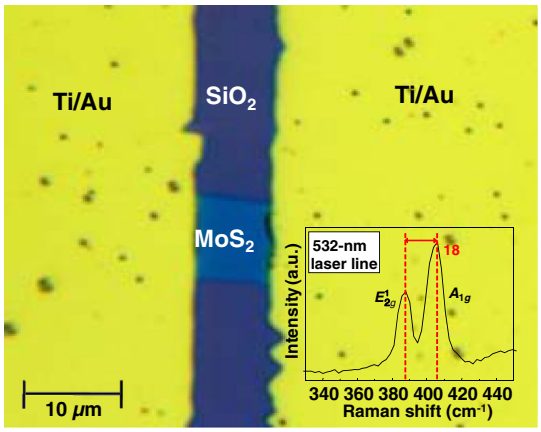

FIG. 3. Microscopic top view of the fabricated monolayer MoS_2 thin-film transistor before the sol-gel passivation process. The inset shows the Raman spectrum of isolated monolayer MoS_2 measured using a laser beam with a wavelength of 532 nm. The difference between the E^1_{2g} and A_{1g} peaks is 18 cm^{-1} that corresponds to monolayer MoS_2 [26].

calculated parameters because the channel interface and the gate oxide are nearly fully trapped with electrons on the application of large positive bias (approximately 30 V), resulting in nearly fully charged interfaces and gate oxide. This full charging minimizes the threshold-voltage shift effect caused by charging in the gate oxide during the measurements. We assume that the trapped charge density near the channel interfaces, oxide-trapped charge density, and threshold voltage (approximately 5 V) are maintained constant during the measurement.

The transfer curves measured at room temperature for different V_{SD} (1 and 10 V) and the corresponding calculated results as functions of the gate overdrive ($V_{GS} - V_{\rm th}$) are shown in Fig. 4(a). Here, $V_{\rm th}$ is determined by the gate voltage at which the drain current is 10^{-12} A. The modeling parameters are the same as in Fig. 2 (Table I). Generally, the

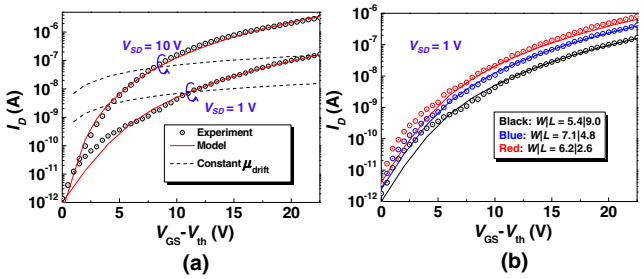

FIG. 4. (a) Experimental and calculated transfer curves as functions of the gate overdrive ($V_{GS} - V_{\rm th}$) for $V_{SD} = 1$ and 10 V. The model parameters are the same as in Table I. The dotted lines are plotted to show the inability of the constant mobility model to explain the measured transfer curves. (b) Transfer-curve comparisons between the models and experiments for different channel widths (W) and lengths (L) at $V_{SD} = 1$ V. The model parameters are the same as in Fig. 4(a).

TABLE I. Parameters for the model.

W (μm)	L (μm)	d (nm)	ε (SiO_2)	$n_{\rm IT}$ (cm^{-2})	t (nm)	g	$m*$ [13]
5.4	9.0	300	$3.9\varepsilon_0$	6×10^{14}	0.8	2	$0.483m_0$

$n_{\rm IT}$ is obtained by means of a relatively accurate interface-trap measurements such as charge pumping, but for the monolayer MoS_2 channel case, because of the nature of the MoS_2 channel close to two dimensions, we cannot use the charge-pumping method that requires channel inversion or accumulation conversion, so we use the swing of the transfer curve in Fig. 4(a) to estimate the value of interface-trap density ($n_{\rm IT}$). In general, the swing of the transfer curve has the following relationship [27]

$$\text{Swing} \cong \ln 10 \frac{kT}{C_{\rm ox}}(C_{\rm ch} + C_{\rm IT}), \tag{10}$$

where $C_{\rm ox}$, $C_{\rm ch}$, and $C_{\rm IT}$ are the gate oxide capacitance per unit area ($=\varepsilon/d$), channel capacitance per unit area (obtained by the permittivity and thickness ratio of the monolayer MoS_2 channel), and capacitance by interface traps per unit area ($=en_{\rm IT}$) respectively. From the transfer curve, we can see that the swing is about 1000 mV/decade, which means that $C_{\rm IT}$ is much larger than $C_{\rm ch}$, and $n_{\rm IT}$ should have order of 10^{14} (cm^{-2}) that is consistent with the value used in the calculation (Table I).

As can be seen in Fig. 4(a), the experimental and calculated results are consistent even for different V_{SD} and for a wide range of I_D up to the order of 10^7 (from 10^{-12} to 10^{-5} A). For comparison, we also plot the transfer curves with the constant drift mobility (0.1 cm/V s) showing huge deviations from the experimental curves. This result shows that in the monolayer TMDC TFT, because the rates of the carrier scattering by interface-trapped charges are maximized due to the proximity between the carriers and the trapped charges, the transfer-curve characteristics cannot be described using the conventional MOSFET model with either constant or field-dependent mobility. Thus, we conclude that in the case of severe interface-charge scattering in the TMDC TFT, the drift mobility should be considered as a function of the carrier (gate bias) and effective interface-trapped charge densities. Then it is possible that the interface-trapped charge densities are extracted from conventional transfer curves instead of much more complicated and expensive interface-trap-density measurement methods such as charge-pumping, capacitance-voltage, high-frequency measurements, and so forth [27]. In Fig. 4(b), we further show comparisons with experimental transfer curves for an additional two width and length pairs (7.1 and 4.8, and 6.2 and 2.6) at $V_{SD} = 1$ V measured at room temperature. The overall consistency can be noticed in this figure with some minute deviations for different widths and lengths other than the

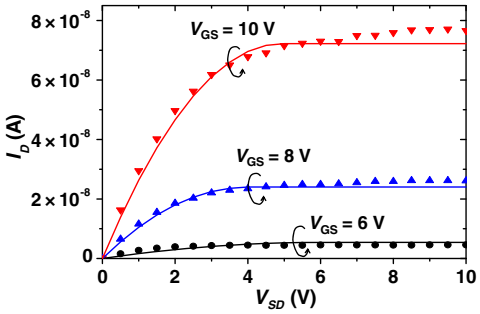

FIG. 5. Output curve comparisons between the models and experiments for $V_{GS} = 6$, 8, and 10 V. The model parameters are the same as in Table I.

previously matched width and length combination (5.4 and 9.0), which we can postulate might mainly originate from the n_{IT} variance among the devices.

As can be noticed in Fig. 4, the experimental results show larger subthreshold swings than the model at lower V_G. This is probably because some portion of the electrons are captured to partially fill the interface traps. As V_G increases, all the traps become completely filled to a constant trap density and then appear to be the model assumption.

We also validate our model for output curve responses for several V_{GS}'s as shown in Fig. 5. For the model results, the data after the saturation point [$V_{SD} \sim (V_{GS} - V_{th})$] are plotted as constant lines, and the model parameters are the same as in Table I. As can be seen in the figure, although there are some discrepancies in the saturation region, the model and the experimental results have good agreement with each other, which, again, confirms the validity of the model. Throughout this paper, we ignore the contact resistance of the source and drain in analyzing the TFT experimental results. The reason is that the resistance levels of the channel shown in Figs. 4 and 5 are larger than 1 MΩ, while the typical TFT contact resistances are much smaller than this.

IV. CONCLUSION

In summary, we propose an operation model of a monolayer TMDC TFT with a high density of interface-trapped charges. Calculating the rate of carrier scattering by trapped charges near the channel interfaces, we obtain the drift mobility and the $I_D - V_{GS}$ curve model. The proposed model is consistent with the experimental results of transfer and output characteristics, which cannot be explained using the conventional MOSFET operation model. We hope that the characteristics of any monolayer TMDC TFT can be calculated using this model for any kind of transition metal or chalcogenide if the simulation parameters are selected appropriately corresponding to the adopted materials and device designs.

ACKNOWLEDGMENTS

This work is supported by the National Research Foundation of Korea Grant funded by the Korea government (MEST) (Grant No. 2016R1D1A1B04930601) and a Korea University Grant.

[1] J. Chang, L. F. Register, and S. K. Banerjee, Comparison of ballistic transport characteristics of monolayer transition metal dichalcogenides (TMDs) MX_2 (M = Mo, W; X = S, Se, Te) n-MOSFETs, in *Proceedings of the 2013 International Conference on Simulation of Semiconductor Processes and Devices (SISPAD)* (IEEE, New York, 2013), p. 408.

[2] S. Das, H.-Y. Chen, A. V. Penumatcha, and J. Appenzeller, High performance multilayer MoS_2 transistors with scandium contacts, Nano Lett. **13**, 100 (2013).

[3] S. Das, M. Demarteau, and A. Roelofs, Nb-doped single crystalline MoS_2 field effect transistor, Appl. Phys. Lett. **106**, 173506 (2015).

[4] S. Larentis, B. Fallahazad, and E. Tutuc, Field-effect transistors and intrinsic mobility in ultra-thin $MoSe_2$ layers, Appl. Phys. Lett. **101**, 223104 (2012).

[5] H. S. Lee, S.-W. Min, Y.-G. Chang, M. K. Park, T. Nam, H. Kim, J. H. Kim, S. Ryu, and S. Im, MoS_2 nanosheet phototransistors with thickness-modulated optical energy gap, Nano Lett. **12**, 3695 (2012).

[6] H. Liu, A. T. Neal, and P. D. Ye, Channel length scaling of MoS_2 MOSFETs, ACS Nano **6**, 8563 (2012).

[7] V. Podzorov, M. Gershenson, C. Kloc, R. Zeis, and E. Bucher, High-mobility field-effect transistors based on transition metal dichalcogenides, Appl. Phys. Lett. **84**, 3301 (2004).

[8] R. B. Radisavljevic, A. Radenovic, J. Brivio, i. V. Giacometti, and A. Kis, Single-layer MoS_2 transistors, Nat. Nanotechnol. **6**, 147 (2011).

[9] A. Sanne, R. Ghosh, A. Rai, H. C. P. Movva, A. Sharma, R. Rao, L. Mathew, and S. K. Banerjee, Top-gated chemical vapor deposited MoS_2 field-effect transistors on Si_3N_4 substrates, Appl. Phys. Lett. **106**, 062101 (2015).

[10] Y. Yoon, K. Ganapathi, and S. Salahuddin, How good can monolayer MoS_2 transistors be?, Nano Lett. **11**, 3768 (2011).

[11] S. Kim, A. Konar, W.-S. Hwang, J. H. Lee, J. Lee, J. Yang, C. Jung, H. Kim, J.-B. Yoo, J.-Y. Choi, Y. W. Jin, S. Y. Lee, D. Jena, W. Choi, and K. Kim, High-mobility and low-power thin-film transistors based on multilayer MoS_2, Nat. Commun. **3**, 1011 (2012).

[12] R. Samnakay, C. Jiang, S. Rumyantsev, M. Shur, and A. Balandin, Selective chemical vapor sensing with few-layer MoS_2 thin-film transistors: comparison with graphene devices, Appl. Phys. Lett. **106**, 023115 (2015).

[13] W. S. Yun, S. W. Han, S. C. Hong, I. G. Kim, and J. D. Lee, Thickness and strain effects on electronic structures of transition metal dichalcogenides: 2H-MX_2 semiconductors (M=Mo, W; X = S, Se, Te), Phys. Rev. B **85**, 033305 (2012).

[14] D. Jiménez, Drift-diffusion model for single layer transition metal dichalcogenide field-effect transistors, Appl. Phys. Lett. **101**, 243501 (2012).

[15] J. Chang, Simulation of channel orientation dependent transport in ultra-scaled monolayer MoX_2 ($X = S$, Se, Te) n-MOSFETs, J. Phys. D **48**, 145101 (2015).

[16] N. Ashcroft and N. Mermin, *Solid State Physics* (Thomson Learning, London, 1976).

[17] M. Lundstrom, *Fundamentals of Carrier Transport* (Cambridge University Press, Cambridge, England, 2009).

[18] T. Ando, A. B. Fowler, and F. Stern, Electronic properties of two-dimensional systems, Rev. Mod. Phys. **54**, 437 (1982).

[19] J.-Y. Noh, H. Kim, and Y.-S. Kim, Stability and electronic structures of native defects in single-layer MoS_2, Phys. Rev. B **89**, 205417 (2014).

[20] D. Jena, A. C. Gossard, and U. K. Mishra, Dislocation scattering in a two-dimensional electron gas, Appl. Phys. Lett. **76**, 1707 (2000).

[21] C. Ataca and S. Ciraci, Dissociation of H_2O at the vacancies of single-layer MoS_2, Phys. Rev. B **85**, 195410 (2012).

[22] D. Liu, Y. Guo, L. Fang, and J. Robertson, Sulfur vacancies in monolayer MoS_2 and its electrical contacts, Appl. Phys. Lett. **103**, 183113 (2013).

[23] J.-H. Hur and S. Jeon, Dislocation scatterings in p-type $Si_{1-x}Ge_x$ under weak electric field, Nanotechnology **26**, 495201 (2015).

[24] F. Gamiz, J. Roldan, J. Lopez-Villanueva, P. Cartujo-Cassinello, and J. Carceller, Surface roughness at the Si-SiO_2 interfaces in fully depleted silicon-on-insulator inversion layers, J. Appl. Phys. **86**, 6854 (1999).

[25] Y. Taur and T. H. Ning, *Fundamentals of Modern VLSI Devices* (Cambridge University Press, Cambridge, England, 2013).

[26] H. Li, Q. Zhang, C. C. R. Yap, B. K. Tay, T. H. T. Edwin, A. Olivier, and D. Baillargeat, From bulk to monolayer MoS_2: Evolution of Raman scattering, Adv. Funct. Mater. **22**, 1385 (2012).

[27] D. K. Schroder, *Semiconductor Material and Device Characterization* (John Wiley & Sons, New York, 2006).